Bioactive Materials 48 (2025) 29–42

Contents lists available at ScienceDirect

Bioactive Materials

journal homepage: www.keaipublishing.com/en/journals/bioactive-materials

Targeted codelivery of nitric oxide and hydrogen sulfide for enhanced antithrombosis efficacy

Weiliang Deng [a,1], Zhixin Xu [a,1], Tong Hua [a,1], Guangbo Ji [a], Zihang Wang [b], Pei Liu [a], Yupeng Zhang [a], Shuo Li [b], Yuqiu Chao [b], Meng Qian [a,**], Qiang Zhao [a,c,*], Jinwei Tian [b,***]

[a] State Key Laboratory of Medicinal Chemical Biology, Key Laboratory of Bioactive Materials (Ministry of Education), Frontiers Science Center for Cell Responses, College of Life Sciences, Nankai University, Tianjin, 300071, China
[b] Department of Cardiology, The Second Affiliated Hospital of Harbin Medical University, Heilongjiang Provincial Key Laboratory of Panvascular Disease, Harbin, 150086, China
[c] The Institute of Cardiovascular Sciences, School of Basic Medical Sciences, State Key Laboratory of Vascular Homeostasis and Remodeling, Health Science Center, Peking University, Beijing, 100191, China

ARTICLE INFO

Keywords:
Nitric oxide
Hydrogen sulfide
Precise delivery
Synergistic effect
Thrombosis

ABSTRACT

Thrombosis is a leading cause of mortality worldwide. As important gaseous signaling molecules, both nitric oxide (NO) and hydrogen sulfide (H_2S) demonstrate antiplatelet and anticoagulant functions, but little attention has been given to their synergistic effect and the underlying mechanism. In the present study, we developed an NO/H_2S codelivery system based on enzyme prodrug therapy (EPT) strategy in which the prodrugs are specifically recognized by the engineered β-galactosidase. Targeted codelivery of NO and H_2S *in vivo* was demonstrated by near-infrared fluorescence imaging and confirmed by measuring plasma and tissue levels; as a result, the side effects caused by systemic delivery, such as bleeding time, were reduced. Delivery of an optimized combination of NO and H_2S with a low combination index (CI) results in a synergistic effect on the inhibition of platelet adhesion and activation. Mechanistically, NO and H_2S cooperatively enhance the cGMP level through redox-based posttranslational modifications of phosphodiesterase 5A (PDE5A), which leads to activation of the cGMP/PKG signaling pathway. Furthermore, targeted codelivery of NO and H_2S demonstrates enhanced therapeutic efficacy for thrombosis in two mouse models of $FeCl_3$-induced arterial thrombosis and deep vein thrombosis. Collectively, these results confirm the synergistic efficacy of NO and H_2S for antithrombotic therapy, and the codelivery system developed in this study represents a promising candidate for clinical translation.

1. Introduction

A thrombus forms when blood coagulates within blood vessels, increasing the individual's risk of severe cardiovascular events such as heart attack, stroke, and pulmonary embolism, each of which can be life-threatening [1,2]. Despite tremendous advances in elucidating the mechanisms mediating platelet function and thrombosis, challenges remain regarding the lack of effective therapeutic strategies for clinical use [3,4]. Thrombosis is a complex, multifactorial process, and identification of key factors of thrombosis is crucial for developing safer and more effective antithrombotic strategies [5–7].

Nitric oxide (NO) and hydrogen sulfide (H_2S) are both important gaseous signaling molecules in the cardiovascular system. In addition to the known vasodilation effect [8], NO also functions as an effective anticoagulant [9]. In the intact vessel, NO is primarily released by the endothelium, which can inhibit the adhesion, aggregation, and activation of platelets, thereby suppressing thrombus formation [10]. The deficiency of endothelium-derived NO is closely linked with thrombotic diseases, whereas supplementation of exogenous NO has demonstrated beneficial effect on anticoagulation [11–13]. In contrast, the potential

Peer review under the responsibility of KeAi Communications Co., Ltd.
* Corresponding author. State Key Laboratory of Medicinal Chemical Biology, Key Laboratory of Bioactive Materials (Ministry of Education), Frontiers Science Center for Cell Responses, College of Life Sciences, Nankai University, Tianjin, 300071, China.
** Corresponding author.
*** Corresponding author.
E-mail addresses: 13821705466@163.com (M. Qian), qiangzhao@nankai.edu.cn (Q. Zhao), tianjinweidr2009@163.com (J. Tian).
[1] Deng W, Xu Z, and Hua T equally contributed to this study.

https://doi.org/10.1016/j.bioactmat.2025.02.012
Received 19 December 2024; Received in revised form 25 January 2025; Accepted 6 February 2025
Available online 13 February 2025

role of H_2S in the regulation of coagulation and thrombosis remains unclear [14,15]. Although some studies have suggested that H_2S can inhibit platelet activation and thrombus formation [16–19], the dosage of H_2S donors utilized varies greatly. More importantly, the mechanism of its antiplatelet effect remains poorly understood. In addition, H_2S has been shown to promote platelet aggregation when it is utilized for treating hyperhomocysteinemia [20]. Furthermore, NO and H_2S engage in cross-talk at both chemical and biological levels [21,22], thereby demonstrating a synergistic effect in various processes of cardiovascular diseases, including angiogenesis and cardioprotection [22,23]. Up to now, limited attention has been paid to the cooperative effect of NO and H_2S in the suppression of thrombus formation.

Cyclic guanosine-3′,5′-monophosphate (cGMP) is a key regulator of platelet activation. The intracellular cGMP pools of platelets are tightly regulated by a fine balance between the activities of NO-stimulated soluble guanylate cyclase (sGC) and phosphodiesterases (PDEs) [24]. NO can activate sGC, leading to an increase in cGMP levels, which activates protein kinase G (PKG) and promotes the phosphorylation of numerous proteins that are responsible for platelet inhibition [10]. Phosphodiesterase type 5 (PDE5A) is a cGMP-specific member of the PDE family. The inhibition or elimination of PDE5A in platelets can increase intracellular cGMP levels, thereby reducing platelet activation and thrombus formation [24,25]. The activity of PDE5A is regulated by redox-based posttranslational modifications that target cysteine residues of proteins. Accumulating evidence has demonstrated that both S-nitrosylation and S-sulfhydration can mitigate the activity of PDE5A [26,27]. In addition, platelet activation is associated with the overproduction of reactive oxygen species [28], which can shift the cysteine residues to a higher oxidation state and reduce the likelihood of S-nitrosylation modification by NO. However, as a reducing agent, H_2S can restore the reactivity of the oxidized cysteine residues and increase the probability of S-nitrosylation modification [22,29]. Therefore, it is reasonable to hypothesize that NO and H_2S may have a synergistic effect on modulating intracellular cGMP levels and thus affect the function and activity of platelets.

The physiological functions of NO and H_2S are intricately related to their concentrations, duration of action, and spatiotemporal distribution [30,31]. Therefore, the precise delivery of appropriate doses of NO or H_2S to target sites is crucial for preclinical research and clinical applications. Previously, we developed an enzyme-prodrug delivery system based on the "bump-and-hole" strategy, and targeted delivery of NO *in vivo* has been achieved by manipulating the biodistribution of engineered β-galactosidase (A4-β-Gals^{H363A}) with reduced side effects due to systemic NO delivery [32]. In this study, we further developed a NO/H_2S codelivery system with the aid of engineered A4-β-Gals^{H363A} and MeGal-protected prodrugs (MeGal-NO and MeGal-H_2S) (Fig. 1). The synergistic effect of NO and H_2S on the suppression of platelet adhesion and activation was evaluated via *in vitro* assays, and the underlying mechanism was investigated. Furthermore, the therapeutic efficacy of the NO/H_2S codelivery system for the treatment of thrombotic diseases was fully assessed using a $FeCl_3$-induced carotid artery thrombosis model and a deep vein thrombosis model.

2. Results

2.1. Construction and in vitro characterization of the NO/H_2S codelivery system

Previously, a targeted NO delivery system was developed via modification of an enzyme–prodrug pair using a 'bump-and-hole' strategy [32]. As a result, a "bumpy" NO donor, MeGal-NO, which was designed by introducing a methyl group at the O6 position of galactosyl-NONOate (Gal-NO), can be specifically recognized by an engineered β-galactosidase (A4-β-Gals^{H363A}). In parallel, we synthesized a MeGal-protected H_2S prodrug (MeGal-H_2S) on the basis of the H_2S donor carbonyl sulfide (COS). As shown in Fig. 2a, MeGal-H_2S releases the H_2S donor (COS)

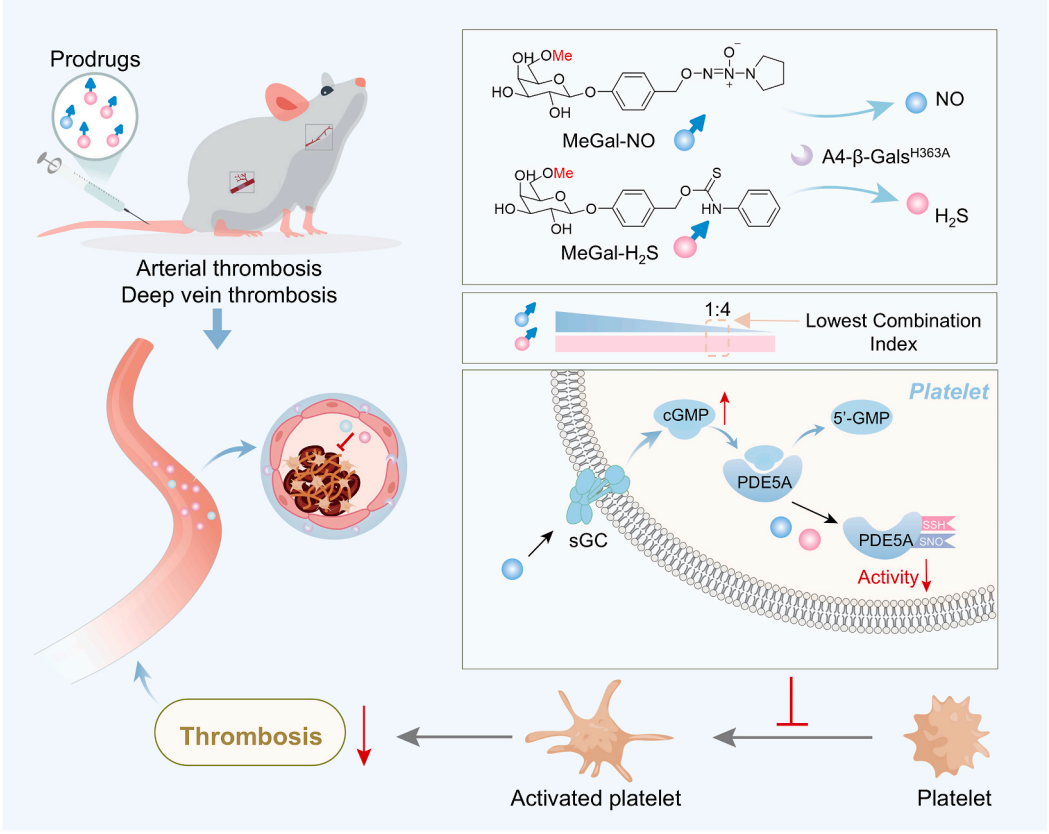

Fig. 1. Schematic illustration shows targeted co-delivery of NO and H_2S enhances the therapeutic efficacy for thrombosis.

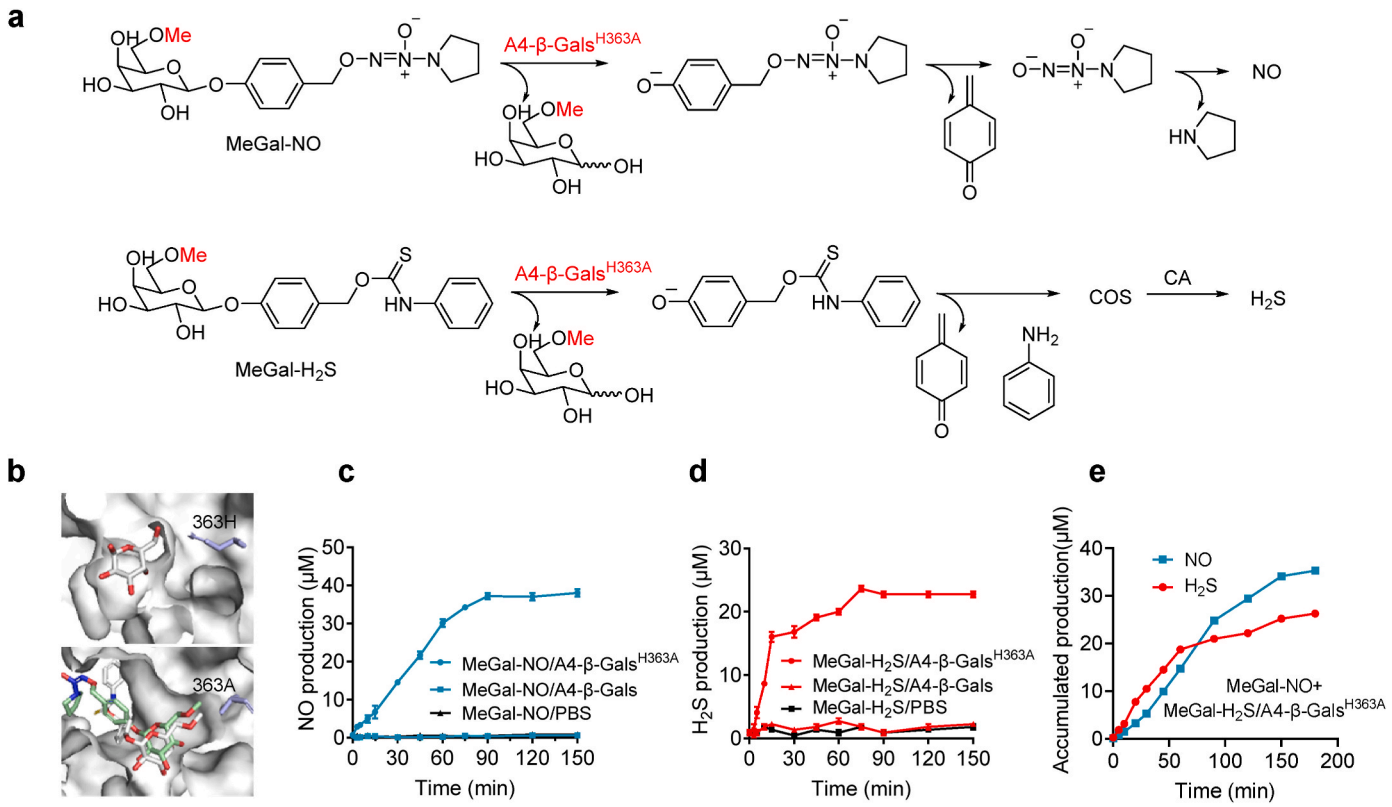

Fig. 2. Synthesis and evaluation of MeGal-NO and MeGal-H_2S prodrugs. (a) Shown is the mechanism of NO and H_2S release from the respective prodrugs (MeGal-NO and MeGal-H_2S) catalyzed by the engineered β-galactosidase A4-β-Gals^{H363A}. (b) Active pocket of wild-type β-galactosidase (PDB code: 1KWK) is shown (left). MeGal-NO (green, shown in stick mode) and MeGal-H_2S(grey, shown in stick mode) were docked into the active pocket of A4-β-Gals^{H363A} using Autodock vina (right). (c, d) *In vitro* release of NO and H_2S from MeGal-NO (50 μM), MeGal-H_2S (50 μM) under different conditions, was measured by Griess (c) and methylene blue (d) assay, respectively. (e) Shown is the *in vitro* release of NO and H_2S simultaneously from the combination of MeGal-NO (50 μM) and MeGal-H_2S (50 μM) under the catalysis of A4-β-Gals^{H363A}. All Data are presented as mean ± SEM (n = 3).

under the catalysis of A4-β-Gals^{H363A}, which can be converted to H_2S by the abundant carbonic anhydrase (CA) *in vivo*. To identify the specific recognition of the prodrugs by A4-β-Gals^{H363A}, a molecular docking experiment was performed (Fig. 2b). Compared with wild-type β-galactosidase, A4-β-Gals^{H363A} has an expanded active pocket that can accommodate the MeGal moiety, and both MeGal-NO and MeGal-H_2S exhibit similar binding modes with A4-β-Gals^{H363A}, suggesting similarities in the release mechanisms.

A4-β-Gals^{H363A} was expressed in *E. coli* BL21 (DE3) and identified via Western blotting (Supplementary Fig. 1). The *in vitro* release of NO and H_2S from MeGal-NO and MeGal-H_2S was subsequently evaluated via Griess and methylene blue assays, respectively. MeGal-NO was efficiently recognized and converted by A4-β-Gals^{H363A}, with a cumulative NO release of approximately 39.02 μM after 150 min, while negligible release was observed in the presence of wild-type β-galactosidase (Fig. 2c). Similarly, MeGal-H_2S (50 μM) remained stable in the presence of wild-type β-galactosidase and carbonic anhydrase, whereas in the presence of A4-β-Gals^{H363A} and carbonic anhydrase, a noticeable release of H_2S was observed, with a cumulative production of approximately 23.18 μM (Fig. 2d). Overall, the release efficiencies of the prodrugs were comparable to those of the previously described donors [33,34]. Furthermore, the codelivery behavior of NO and H_2S was evaluated by coincubating equal amounts of MeGal-NO and MeGal-H_2S with A4-β-Gals^{H363A}. The release profile of MeGal-NO and MeGal-H_2S remained almost unchanged when they were administered in combination (Fig. 2e), which may facilitate the fine tuning of the codelivery of NO and H_2S. Furthermore, the sustained and controlled delivery of NO and H_2S *in vivo* can be achieved by carefully selecting the concentration of enzyme and prodrug pairs [35].

2.2. *In vivo evaluation of the NO/H_2S codelivery system*

To achieve stable and sustained *in vivo* catalytic activity, A4-β-Gals^{H363A} was encapsulated in a hyaluronic acid methacryloyl (HAMA) hydrogel and injected into the targeted site, as depicted in Fig. 3a. *In vitro* assessments demonstrated that hydrogel encapsulation did not affect the catalytic activity of A4-β-Gals^{H363A} compared with when they were dissolved in solution (Supplementary Fig. 2). To obtain further insight into the *in vivo* catalytic activity of the A4-β-Gals^{H363A}-loaded hydrogel, *in vivo* imaging was performed by using a near-infrared fluorescence probe (MeGal-DDSY). When the A4-β-Gals^{H363A}-loaded hydrogel was injected around the left carotid artery followed by intravenous administration of MeGal-DDSY, a remarkable increase in fluorescence intensity was observed at the site where the hydrogel was implanted (Fig. 3b).

For *in vivo* imaging of H_2S release, a H_2S-responsive near-infrared fluorescence probe (H_2S-DDSY) was loaded with A4-β-Gals^{H363A} into the HAMA hydrogel, which was then injected around the left carotid artery of each mouse. After 12 h, a fluorescence signal was detected at the targeted site, representing endogenous H_2S production by vascular tissues (Fig. 3c). Subsequently, MeGal-H_2S was administered intravenously, and the fluorescence intensity evidently increased after 10 min, suggesting the successful conversion of MeGal-H_2S into H_2S *in vivo* through the catalysis of local A4-β-Gals^{H363A}.

Electron paramagnetic resonance (EPR) was employed to quantify the NO generation *in vivo*. The A4-β-Gals^{H363A}-loaded hydrogel was implanted around the left carotid artery, followed by intravenous injection of MeGal-NO. Compared with that of the right carotid artery, a notable increase in the characteristic triplet EPR spectrum of $(DETC)_2Fe$-

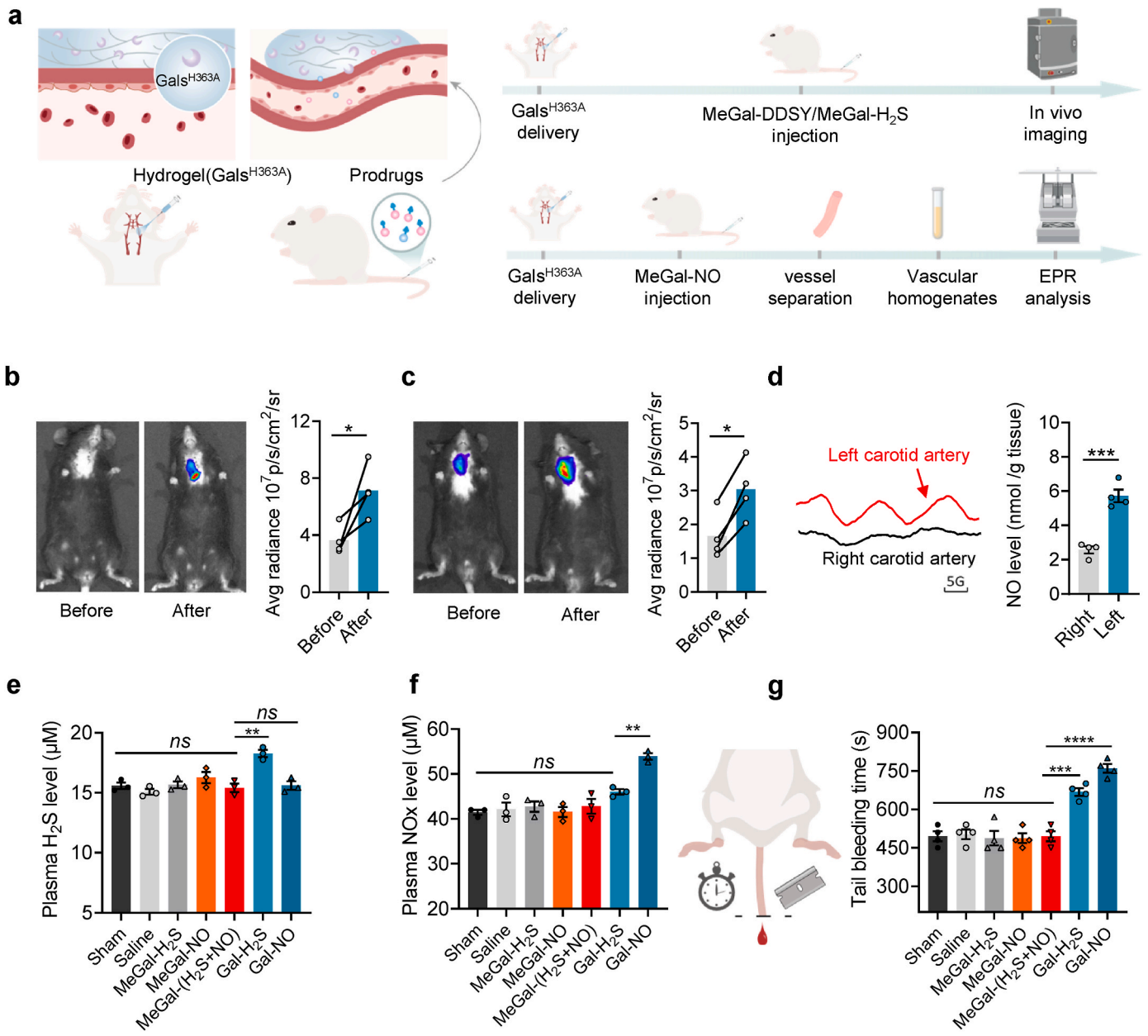

Fig. 3. Targeted co-delivery of NO and H_2S was evaluated *in vivo*. (a) Schematic illustration shows the delivery and detection of H_2S and NO. (b) *In vivo* imaging shows the specific and efficient hydrolysis of MeGal-DDSY in response to engineered β-galactosidase A4-β-Gals^{H363A} administrated around the carotid artery (n = 4). (c) *In vivo* imaging shows the targeted release of H_2S (n = 4). (d) NO levels of the carotid arteries with and without implantation of enzyme-loaded hydrogel were compared by electron paramagnetic resonance (EPR) analysis. Shown are EPR spectra (left) and the quantitative analysis of NO production (right) (n = 4). (e, f) The plasma H_2S and NOx levels were detected by methylene blue assay and chemiluminescence, respectively (n = 3). (g) Tail bleeding time was evaluated after different treatments (n = 4). All data are presented as mean ± SEM. $^*p < 0.05$, $^{**}p < 0.01$, $^{***}p < 0.001$, $^{****}p < 0.0001$, *ns*, $p > 0.05$.

NO ($a_N = 12.78$ G, $g_{iso} = 2.041$) was observed after the administration of MeGal-NO. The quantitative results also revealed a 2.23-fold increase in the NO level (Fig. 3d).

The plasma levels of H_2S and NOx were then detected. Compared with the sham group, the targeted delivery of H_2S and/or NO did not cause an increase in the systemic levels of H_2S and NO (Fig. 3e and f). In contrast, systemic delivery of NO or H_2S using donors (Gal-NO or Gal-H_2S) controlled by endogenous β-galactosidases resulted in a remarkable increase in plasma NOx or H_2S levels. Given that antithrombotic therapy may induce side effects such as bleeding [4], the coagulation function of mice after various treatments was assessed. As shown in Fig. 3g, there was no significant difference in bleeding time following targeted delivery of H_2S, NO, or their combination compared with the sham group. However, systemic delivery of NO or H_2S evidently prolonged bleeding time in mice, which may increase the risk of bleeding symptoms (Fig. 3e).

2.3. NO and H_2S cooperatively inhibit platelet adhesion and activation

Platelets are anucleate blood cells produced by megakaryocytes and are closely related to physiological hemostasis and pathological thrombosis [36]. Collagen, one of the major components exposed after vascular injury, is capable of inducing platelet adhesion and activation. We coated glass slides with collagen for a platelet adhesion assay, and the purity of extracted platelets was verified by flow cytometry (Fig. 4a, Supplementary Fig. 3). The inhibitory effect of NO was assessed by

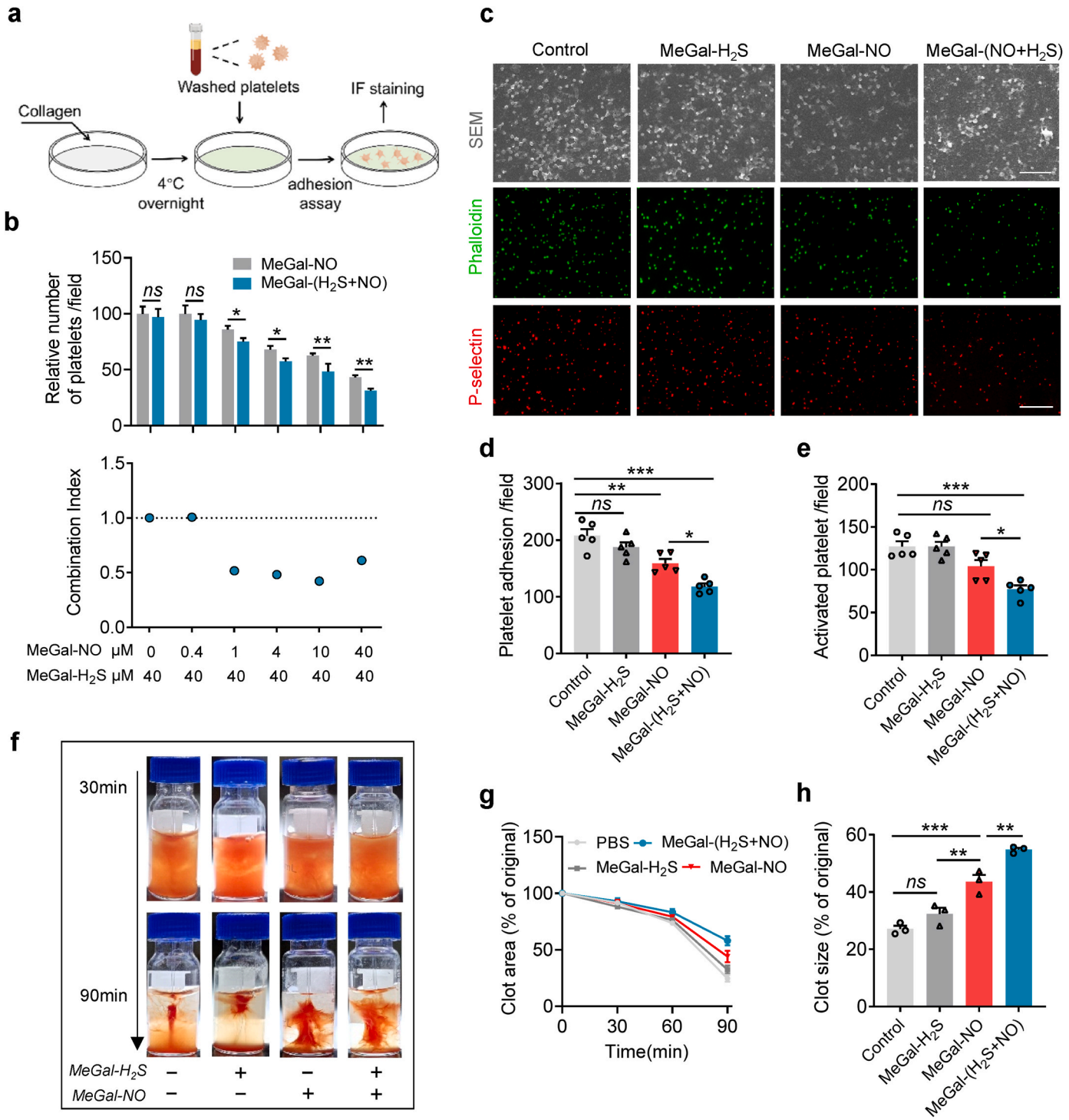

Fig. 4. NO and H_2S cooperatively inhibit platelet adhesion and activation. (a) Schematic diagram shows platelet adhesion assay. (b) Platelets of equal quantity were incubated with indicated concentrations of prodrugs in the present of A4-β-Gals^{H363A} (0.05 mg/mL), respectively. Relative number of platelets were measured and normalized to the control values (top). Combination index (CI) was calculated by using CompuSyn software (bottom), and synergistic effect between two drugs was observed at CI < 1. (c) Representative SEM images show platelets on the surface of collagen (top). CLSM images show phalloidin-stained platelets (middle) and P-selectin^{+} activated platelets (Bottom) in response to different treatments (PBS, 40 μM H_2S, 10 μM NO, and 40 μM H_2S combined with 10 μM NO), Scale bars = 20 μm for SEM; Scale bars = 10 μm for CLSM. (d, e) Phalloidin+ and p-selectin + platelets were further quantified (n = 5). (f) Clot retraction was triggered after addition of thrombin (1 U/mL), and platelets of equal quantity were incubated with H_2S (40 μM) and NO (10 μM) individually or in combination, respectively. Representative images at 30 and 90 min are shown. (g, h) The clot area (%) (g) and the two-dimensional size of the clot (h) were further quantified based on the images (n = 4). All Data are presented as mean ± SEM. $^{*}p < 0.05$, $^{**}p < 0.01$, $^{***}p < 0.001$, *ns*, $p > 0.05$.

quantifying the adherent platelets, and with increasing NO concentration (0.4 μM–40 μM), the quantity of adherent platelets gradually decreased, indicating a dose-dependent inhibitory effect of NO on platelet adhesion.

Next, we sought to investigate whether H_2S and NO had a synergistic effect on mitigating platelet adhesion. At a concentration of 40 μM, H_2S had no detectable effect on platelet adhesion (Fig. 4b). Interestingly, the addition of H_2S (40 μM) markedly enhanced the inhibitory effect of NO on platelet adhesion with a low combination index (CI) in certain combinations (NO:H_2S = 1:40, 4:40, 10:40, 40:40 μM), indicating a synergistic effect (Fig. 4b). The optimized concentration combination with the lowest CI (NO:H_2S = 10:40 μM) was subsequently utilized for further investigation. The synergistic effect on platelet adhesion was further verified by scanning electron microscopy (SEM) and cytoskeletal staining (Fig. 4c). The results indicated that codelivery of NO and H_2S led to a more pronounced decrease in platelet adhesion than treatment with NO or H_2S alone (Fig. 4d). Additionally, combined treatment resulted in a notable reduction in the quantity of P-selectin$^+$ (a marker of activated platelets) platelets (Fig. 4e), suggesting a synergistic effect of NO and H_2S that prevents platelet activation.

Activated platelets extend filopodia and lamellipodia, and the fibrin fibers are pulled together by the platelets to retract the clot. As shown in Fig. 4f, blood clots in each of the groups gradually contracted and eventually converged at the central position. However, compared with that in the control group and the H_2S-treated group, the clot area in the NO-treated group was markedly greater, indicating that NO effectively

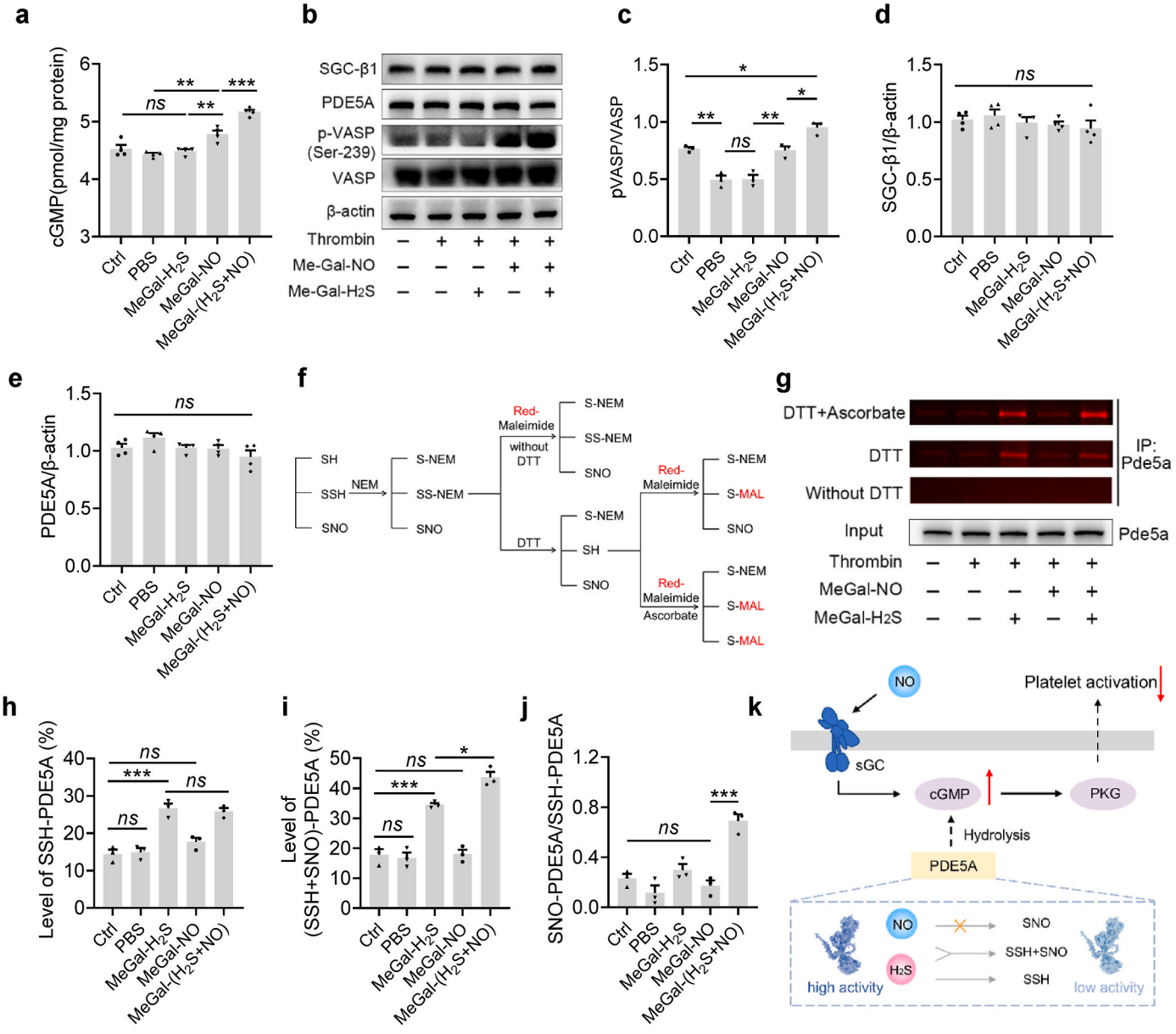

Fig. 5. NO and H_2S cooperatively enhance cGMP/PKG signaling pathway. (a) Intracellular cGMP levels in platelets stimulated with thrombin (0.05 U/mL) were measured by ELISA. Platelets of equal quantity were treated with H_2S (40 μM), NO (10 μM), or H_2S (40 μM) combined with NO (10 μM), respectively. (b–e) Shown is a Western blot and quantification for expression of sGC-β1, VASP, Phospho-VASP-S239 (p-VASP), and PDE5A in platelets after treated with PBS, H_2S (40 μM), NO (10 μM), or H_2S (40 μM) combined with NO (10 μM), respectively (n = 4). (f) Schematic diagram shows the modified red-maleimide fluors switch protocol. (g) PDE5A was enriched from platelets through immunoprecipitation, and its levels of S-sulfhydration (SSH) and S-nitrosylation (SNO) were detected. (h, i) The ratio of fluorescence intensity to the input of PDE5A was employed to evaluate the levels of SSH-PDE5A (h) or (SSH + SNO)-PDE5A (i). (j)The ratio of SNO-PDE5A to SSH-PDE5A was further calculated. (k) Schematic illustration summarizes the synergistic mechanism of NO and H_2S in the cGMP/PKG signaling pathway. All Data are presented as mean ± SEM. $^*p < 0.05$,$^{**}p < 0.01$, $^{***}p < 0.001$, *ns*, $p > 0.05$.

suppressed platelet activation. The combination of NO and H_2S resulted in the most effective inhibition of clot retraction, demonstrating a markedly reduced clot area in contrast to the other groups (Fig. 4g and h). Collectively, these results indicate that H_2S acts in a synergistic manner with NO to inhibit platelet activation.

2.4. NO and H_2S cooperatively enhance the cGMP/PKG signaling pathway

To gain further insight into the underlying mechanism of the synergistic effect of NO and H_2S on platelet inhibition, platelets were stimulated *in vitro* with thrombin and treated with the NO/H_2S codelivery system. The intracellular levels of cGMP (Fig. 5a), as well as the phosphorylation levels of the PKG substrate vasodilator-stimulated phosphoprotein (VASP), were determined (Fig. 5b and c). Consistent with previous reports [37], stimulation with thrombin did not markedly alter the intracellular cGMP levels but did lead to a decrease in VASP phosphorylation. Conversely, treatment with NO markedly increased intracellular cGMP levels and VASP phosphorylation in platelets. Notably, treatment with H_2S alone did not affect cGMP levels or VASP phosphorylation; however, codelivery of NO and H_2S resulted in further increases in cGMP levels and VASP phosphorylation compared with those in the group treated only with NO.

sGC is the sole enzyme responsible for cGMP production in platelets. Western blot analysis revealed no discernible differences in sGC-β1 expression levels among the groups (Fig. 5d). Furthermore, the inhibition of sGC by 1 H-(1,2,4) oxadiazole(4,3-α) quinoxaline-1-one (ODQ) administration abolished the increase in cGMP levels and VASP phosphorylation induced by NO alone or in combination with H_2S (Supplementary Fig. 4).

The expression of PDE5A, which is a cGMP-specific hydrolytic enzyme present in platelets, remained unchanged following different treatments (Fig. 5e). Sequence analysis via the iCysMod online tool revealed several cysteine modification sites on PDE5A (Supplementary Fig. 5) [38], suggesting that multiple redox-based posttranslational modifications may occur on PDE5A. A modified biotin switch method

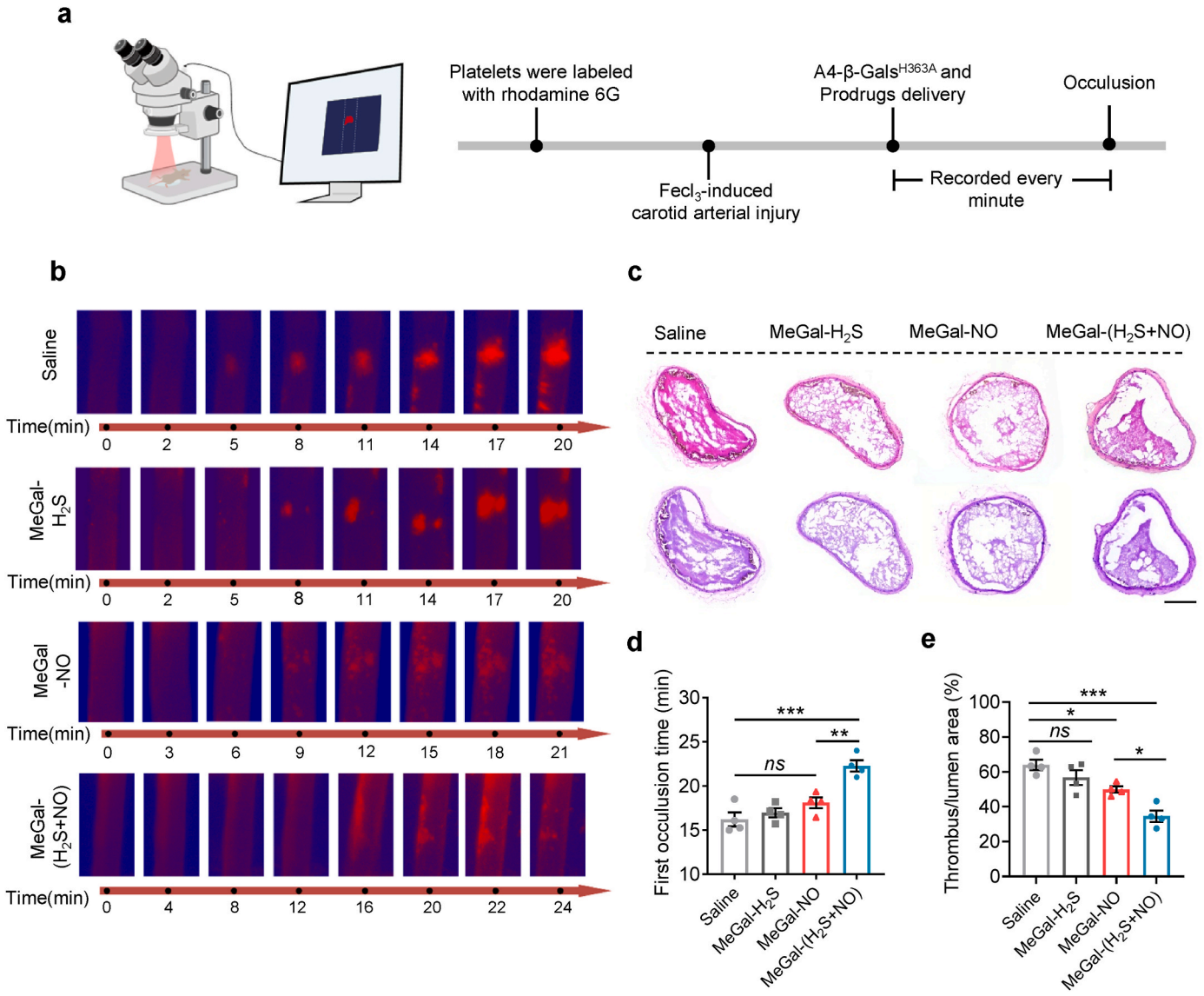

Fig. 6. Targeted delivery of NO and H_2S cooperatively alleviates carotid arterial thrombosis in mice. (a) The experimental schedule is shown for $FeCl_3$-induced carotid arterial thrombosis model. (b) Representative images of thrombosis in carotid artery are shown at different time points, the red part, which represented thrombus. (c) Representative H&E (top) and periodic acid–Schiff (PAS) (bottom) staining on cross-sections of thrombus are shown. Scale bars = 100 μm. (d) The mean time of the first occlusion in mice was measured (n = 4). (e) The ratio of thrombosis cross-sectional area to lumen cross-sectional area was quantified (n = 4). All Data are presented as mean ± SEM. $^*p < 0.05$, $^{**}p < 0.01$, $^{***}p < 0.001$, *ns*, $p > 0.05$.

was subsequently employed to assess the S-sulfhydration levels of PDE5A, as well as the total S-sulfhydration and S-nitrosylation levels (Fig. 5f and g) [22,39]. Stimulation with thrombin did not affect the S-sulfhydration levels of PDE5A, nor did it affect the total S-sulfhydration and S-nitrosylation levels. Treatment with H_2S clearly increased the S-sulfhydration level of PDE5A (Fig. 5h). In contrast, NO did not alter the total S-sulfhydration and S-nitrosylation levels of PDE5A; however, treatment with NO and H_2S in combination resulted in increased total S-sulfhydration and S-nitrosylation levels of PDE5A with a markedly increased proportion of S-nitrosylation (Fig. 5i and j), indicating a synergistic effect of NO and H_2S on the redox-based posttranslational modifications of PDE5A. As both S-nitrosylation and S-sulfhydration downregulated PDE5A activity, the cGMP level increased accordingly (Fig. 5k).

2.5. NO and H_2S cooperatively inhibit $FeCl_3$-induced thrombosis in mice

An $FeCl_3$-induced vascular injury model was utilized to evaluate occlusive thrombosis in this study (Fig. 6a). Upon vascular injury induced by $FeCl_3$, fluorescence signals were detected within the vessel and intensified progressively with increasing thrombus formation (Fig. 6b). Blood flow cessation was observed in all the groups. H&E and PAS staining revealed that the carotid arterial thrombi were composed of fibrin and platelets (Fig. 6c). Compared with saline treatment, H_2S treatment did not affect time to occlusion (Fig. 6d) or thrombus cross-sectional area (Fig. 6e), whereas NO treatment moderately prolonged the average occlusion time and reduced the thrombus cross-sectional area. In contrast, the codelivery of NO and H_2S synergistically reduced $FeCl_3$-induced thrombus formation, as evidenced by the markedly increased time to occlusion and decreased thrombus cross-sectional area (Fig. 6d and e).

2.6. NO and H_2S cooperatively inhibit deep vein thrombosis in mice

The synergistic effect of NO and H_2S on thrombosis was next evaluated in a mouse model of deep vein thrombosis (Fig. 7a). The model was established through inferior vena cava flow reduction, in which a severe thrombus was observed upstream (toward the tail) of the ligated site (Fig. 7b). After 48 h, thrombi were observed in all the groups (Fig. 7c) and were characterized by a dark red color, indicating a high content of red blood cells and fibrin [40]. Both the weights and lengths of the venous thrombi were evidently lower in the mice treated with NO than in those of the saline group and the H_2S group (Fig. 7d and Supplementary Fig. 6), demonstrating the pronounced inhibition of deep vein thrombosis by NO. In the mice treated with NO and H_2S in combination, additional reductions in the weights and lengths of the venous

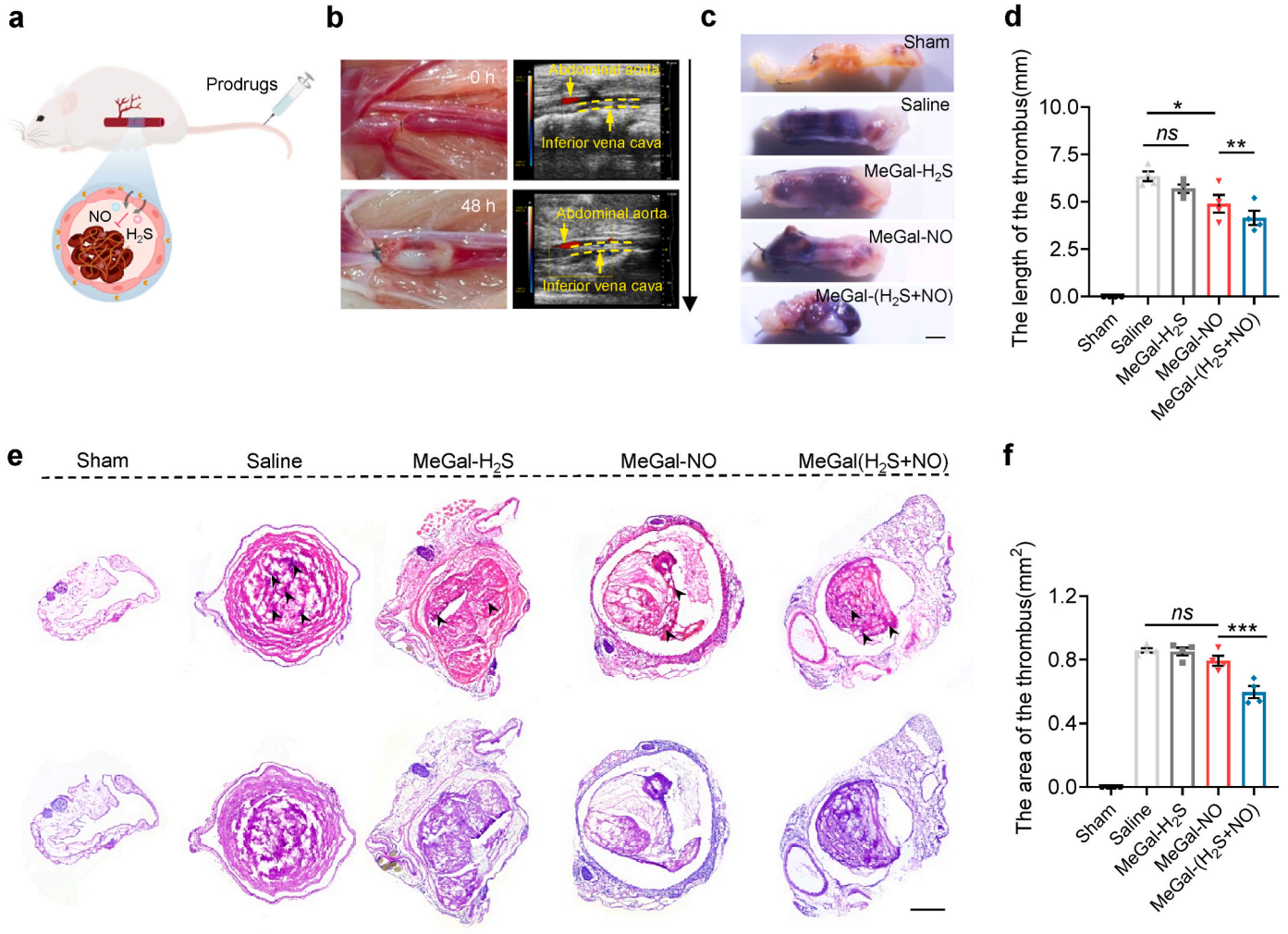

Fig. 7. Targeted delivery of NO and H_2S cooperatively inhibit deep vein thrombosis in mice. (a) Schematic illustration shows deep vein thrombosis model. (b) Shown are representative images of the thrombus and Doppler ultrasound detection at 48 h postoperatively. (c) Representative stereoscopic images of the thrombus are shown. (n = 4), Scale bars: 1 mm. (d) The length of the thrombus in inferior vena cava segment. (e) Representative H&E (top) and PAS (bottom) staining on cross-sections of venous thrombus are shown. The arrows indicate the infiltration of nucleated cells. Scale bars: 100 μm. (f) The cross-section area of the venous thrombus (n = 4). All Data are presented as mean ± SEM. $^*p < 0.05$, $^{**}p < 0.01$, $^{***}p < 0.001$, *ns*, $p > 0.05$.

thrombi were observed.

H&E and PAS staining revealed that, compared with arterial thrombi, venous thrombi contained a greater proportion of nucleated cells, indicating the involvement of neutrophils and macrophages in venous thrombosis (Fig. 7e) [41]. Treatment with NO or H_2S alone did not affect the thrombus area, whereas a notable reduction in the thrombus area was observed in the group treated with a combination of NO and H_2S (Fig. 7f). These results support the synergistic effect of NO and H_2S on the inhibition of deep vein thrombosis.

3. Discussion

Both NO and H_2S are essential gaseous signaling molecules in the human body, and they have similar effects on various biological processes, including vasodilation [42], angiogenesis [23], and cardioprotection [22,43–45]. More importantly, their biological functions are closely related to their concentrations and spatiotemporal distributions; thus, the precise delivery of NO or H_2S to targeted sites is crucial for clinical applications [30,31]. In recent years, interest in the targeted delivery of NO and H_2S has increased [30,31,46–48]. Among targeted delivery methods, the enzyme-prodrug strategy, in which the biodistribution of an enzyme is utilized to precisely control both the location and quantity of drug release, has garnered substantial attention [13,33,49–52]. In our previous study, on the basis of the "bump-and-hole" principle of chemical biology, we developed an enzyme-prodrug NO delivery system that has shown beneficial therapeutic efficacy for different ischemic diseases owing to its targeted delivery profile [32]. In the present study, we developed an NO/H_2S codelivery system capable of the precise release of NO and H_2S both *in vitro* and *in vivo*, providing a robust tool for investigating the biological effects of NO and H_2S.

As an important antithrombotic factor in healthy blood vessels, NO produced by endothelial cells can inhibit platelet adhesion, aggregation, and activation, thereby preventing thrombus formation [53,54]. In the present study, NO inhibited platelet adhesion and activation in a dose-dependent manner. Compared with those of NO, the precise role and relevant mechanism of H_2S regarding platelet inhibition are far from understood, especially the synergistic effect of H_2S in combination with NO [14,15]. In this study, by exploiting an enzyme–prodrug delivery system, the codelivery of NO and H_2S at precisely controlled relative concentrations was achieved. It has been accepted that H_2S fails to inhibit platelet adhesion and activation at normal physiological concentrations [17]; however, H_2S enhances the inhibitory effect of NO on platelets when it is administered in combination with low combination indices. A similar synergistic effect has previously been reported in the case of vasodilation [42].

Cytosolic cGMP levels play crucial roles in platelet inhibition and are finely regulated by the balance between sGC activity and that of PDEs. In the present study, treatment with NO effectively increased intracellular cGMP levels and VASP phosphorylation, which was due to the activation of sGC and subsequently increased generation of cGMP [10]. The effect of H_2S on the intracellular cGMP level is relatively complicated, which may be due to differences in cell types and H_2S donors used [55,56]. Although some studies have shown that H_2S can affect cGMP levels in vascular smooth muscle cells, no significant influence of H_2S on cGMP levels or VASP phosphorylation in platelets was observed in this study. Nevertheless, compared with the group treated only with NO, combined treatment with NO and H_2S resulted in a further increase in cGMP levels and VASP phosphorylation. Since sGC is the sole enzyme responsible for cGMP synthesis in platelets and is activated solely by NO, the synergistic effect of H_2S with NO may be attributed to the inhibition of cGMP hydrolysis. Among the phosphodiesterases expressed in platelets, PDE5A is the primary enzyme responsible for the hydrolysis of cGMP [10]. Both NO and H_2S have been reported to reduce PDE5A activity through S-sulfhydration and S-nitrosylation, respectively, of the multiple reactive cysteine residues of PDE5A [26,27]. In this study, the S-sulfhydration and S-nitrosylation levels PDE5A were assessed via a modified biotin switch method using sulfhydryl-reactive Cy5.5-maleimide, and the results demonstrated that H_2S not only increased the S-sulfhydration level of PDE5A but also promoted the total S-sulfhydration and S-nitrosylation levels of PDE5A. This is ascribed to the oxidation of thiols caused by the reactive oxygen species generated during platelet activation, whereby H_2S can either react directly with the oxidized thiols to complete the S-sulfhydration modification [57] or function as a reducing agent to restore the reactivity of thiols [29], thus enhancing the S-nitrosylation of PDE5A. In contrast, NO cannot react with oxidized thiols (-SOH) to thereafter accomplish the S-nitrosylation of PDE5A [58]. The synergistic effect of NO and H_2S on the modification of cysteine residues has also been reported by other groups [22]. In contrast to our studies, Sun et al. found that H_2S treatment alone can enhance the level of protein S-nitrosylation in ischemic myocardium which could be explained by the discrepancy in pathologic microenvironment between myocardial ischemia and thrombotic diseases. Additionally, considering that the GAF domain (Val156-Gln331) of PDE5A is responsible for cGMP binding [59], the redox-based posttranslational modifications of Cys169, Cys220, and Cys268 may play essential roles in modulating the activity of PDE5A, which needs to be validated by further investigations.

To fully evaluate the antithrombotic effect of the NO/H_2S codelivery system, $FeCl_3$-induced carotid artery thrombosis and deep vein thrombosis models were established in mice. Compared with the systemic administration of NO or H_2S [18,60], a negligible influence on tail bleeding time was observed following targeted delivery of NO or H_2S to the thrombosis site, indicating a reduced impact on the coagulation function of the mice. The targeted delivery of H_2S did not alleviate thrombosis in either of the two models, which is different from the results previously reported regarding systemic administration of H_2S [18]. This is because systemic H_2S administration can modulate various coagulation factors in the blood, including tissue factor pathway inhibitors [61] and fibrinogen [62], thereby resulting in the inhibition of thrombosis. In contrast, targeted delivery of NO effectively inhibited both arterial and venous thrombosis, and synergistic inhibition was observed when NO and H_2S were administered in combination.

In summary, we developed an enzyme–prodrug system for the codelivery of NO and H_2S, and controlled release of NO and H_2S was observed both *in vitro* and *in vivo* under the catalysis of engineered β-galactosidase. Codelivery of NO and H_2S exerts a synergistic effect on platelet adhesion and activation through redox-based posttranslational modifications of PDE5A, leading to upregulation of cGMP/PKG signaling pathway activity. Furthermore, the therapeutic efficacy of this method for thrombosis was evaluated in two mouse models of $FeCl_3$-induced carotid artery thrombosis and deep vein thrombosis, which demonstrated that the codelivery of NO and H_2S is a promising strategy for treating clinical thrombosis-related disorders.

4. Materials and methods

4.1. Materials

Ferric (III) chloride ($FeCl_3$), and *N,N*-dimethyl-p-phenylenediamine were obtained from Xiensi Biochemical Technology Co., Ltd (Tianjin, China). Methanol and ethyl alcohol were obtained from Tianjin Chemical Reagent Company (Tianjin, China). Imidazole, Deferoxamine mesylate salt, and isopropyl β-D-thiogalactoside (IPTG) were obtained from Merck Millipore (Burlington, MA, USA). Rhodamine 6G was obtained from Sigma-Aldrich (St. Louis, MO, USA). DL-Dithiothreitol (DTT), Zinc acetate ($Zn(COO)_2$), *N*-ethylmaleimide and Cy5.5-maleimide were purchased from Aladdin Biochemical Technology Co., Ltd (Shanghai China). Sodium ascorbate was obtained from Alfa Aesar (Haverhill, MA, USA). Peptone, yeast extract, and rhodamine-labeled goat anti-rabbit IgG (A-11012) secondary antibody were purchased from Thermo Fisher Scientific (Waltham, MA, USA). Non-fat powdered milk, collagen, thrombin, bovine serum albumin (BSA), and Periodic

acid-schiff staining (PAS) kit (Cat#G1280) was purchased from Solarbio Science & Technology Co., Ltd (Beijing China). Neocuproine and Selective soluble guanylyl cyclase inhibitor ODQ were sourced from MedChem Express (Monmouth Junction, NJ, USA). Hyaluronic acid methacryloyl (HAMA) hydrogel (Cat#HAMA-150K) was a product of EFL-Tech Co., Ltd (Suzhou, China). Haematoxylin and Eosin (H&E) staining kit (Cat#DH0006) was purchased from Leagene Biotechnology Co., Ltd (Beijing, China). cGMP ELISA Kit (Cat#E-EL-0083) was obtained from Elabscience Biotechnology Co., Ltd (Wuhan, China). Ni-NTA Agarose (AS045), rProtein A/G plus Magpoly beads (RM09008), FITC-conjugated Phalloidin (RM02836), rabbit β-actin antibody (AC038), mouse anti His-tag antibody (AE003), rabbit anti-Phospho-VASP-S239 antibody (AP0187) and rabbit anti-VASP antibody (A0166) were purchased from ABclonal Technology Co., Ltd (Wuhan, China), mouse anti-P-selectin antibody (sc-8419) and mouse anti-PDE5A antibody (sc-136027) was obtained from Santa Cruz Biotechnology Co., Ltd (CA, USA), FITC-CD41a antibody (Cat#133903) was obtained from BioLegend Co., Ltd (CA, USA). Gal-NO and Gal-H_2S were synthesized according to the reported protocol [13,33]. The synthesis of MeGal-NO and MeGal-H_2S, and fluorescence probes MeGal-DDSY and H_2S-DDSY were described in **Supplementary materials**.

4.2. In vitro release of MeGal-NO and MeGal-H_2S

In vitro NO release was determined using the Griess kit assay. 50 μM of MeGal-NO was dissolved in PBS buffer (pH 7.4), and simultaneously, A4-β-Gals^{H363A} was put into the solutions at a concentration of 0.005 mg/mL. At each predetermined time interval, 50 μL of the reaction mixture was transferred to a 96-well plate. Subsequently, 50 μL of Griess A and 50 μL of Griess B were added, followed by immediate measurement of the absorbance at a wavelength of 540 nm using an Enspire microplate reader (PerkinElmer LLC, USA).

In vitro release of H_2S was determined by the methylene blue method. MeGal-H_2S was dissolved in PBS buffer (pH 7.4) (50 μM), and A4-β-Gals^{H363A} and carbonic anhydrase (CA) were added at concentrations of 0.005 and 0.025 mg/mL, respectively. At the designated time points, 50 μL of the reaction mixture was transferred to a 96-well plate, followed by the sequential addition of 10 μL of $Zn(COO)_2$ solution (1 %, w/v), 20 μL of $FeCl_3$ solution (30 mM, dissolved in 1.2 M HCl), and 20 μL of N,N-dimethyl-*p*-phenylenediamine (20 mM, dissolved in 7.2 M HCl), and finally the absorbance was measured at 670 nm wavelength.

4.3. Molecular docking of A4-β-Gals^{H363A} with prodrugs

The 3D structures of MeGal-NO and MeGal-H_2S were both drawn using ChemDraw 3D software and subjected to energy minimization before docking. Using the X-ray crystal structure of the wild-type β-galactosidase (PDB: 1KWK) as a template [63], homology modeling of A4-β-Gals^{H363A} was performed using the Swiss-model online tool [64], and the crystal structure with the highest score was selected. Before docking, the crystal water molecules were removed from the protein, while retaining all rotatable bonds in the ligand molecules. Referring to the binding site of wild-type β-galactosidase, the docking center of the A4-β-Gals^{H363A}was set as x = 24, y = 10, z = 28, and the box size was set as x = 40, y = 40, z = 40. The optimal binding mode was determined based on the docked conformation with the lowest free energy.

4.4. Expression and purification of A4-β-Gals^{H363A}

A4-β-Gals^{H363A} was expressed in *E. coli* BL21(DE3). Bacteria were cultured in LB medium containing 100 μg/mL ampicillin. When the OD_{600} of the culture reached 0.8, induction was carried out by adding 0.1 mM isopropyl β-D-1-thiogalactopyranoside (IPTG), and then the culture temperature was set to 18 °C for a further 12 h. The cells were then harvested by centrifugation at 8000 rpm for 15 min to remove the medium, followed by bacterial cell lysis using sonication. The cell lysate was collected after centrifugation at 12000 rpm for 10 min. The A4-β-Gals^{H363A} containing a His-tag was purified using Ni-NTA. Washing buffer (30 mM imidazole, 200 mM KCl, 20 mM Tris-HCl, pH 8.0) was used for removing impurities, and elution buffer (300 mM imidazole, 200 mM KCl, 20 mM Tris-HCl, pH 8.0) was used for competitive elution of A4-β-Gals^{H363A}. The eluted protein was further identified by Western blot. The purified A4-β-Gals^{H363A} was concentrated using a 40 kDa ultrafiltration tube (Millipore Inc, USA), and the solvent was replaced with PBS.

4.5. Animals

C57BL/6 mice (male, 8 weeks old) and Sprague-Dawley rats (male, 8 weeks old) were purchased from Vital River Laboratory Animal Technology (Beijing, China). Animals were randomly divided into treatment and control groups. All experiments and animal procedures were approved by the Animal Experiments Ethical Committee of Nankai University and conducted in accordance with the *Guide for Care and Use of Laboratory Animals.*

4.6. In vivo detection of A4-β-Gals^{H363A} activity and H_2S release

Specifically, C57BL/6 mice were initially anesthetized by inhalation of a mixed isoflurane at a concentration of 3 %, which was then maintained at 1.5 % throughout the experimental process. The limbs of the mice were immobilized on the operating table, and the fur on the neck was shaved. An incision of 1 cm was made along the midline of the neck, and the left carotid artery was separated. Subsequently, 20 μL of HAMA hydrogel containing A4-β-Gals^{H363A} (0.005 mg/mL) was injected around the carotid artery. Finally, the incision was closed using 6-0 nylon sutures (Ling Qiao, Ningbo, China).

The fluorescence probe MeGal-DDSY was used for assessing the enzymatic activity of A4-β-Gals^{H363A} *in vivo*. During the experiments, mice were anesthetized with isoflurane, and 100 μL of MeGal-DDSY (0.1 mg/mL) was injected via the tail vein. Similarly, the fluorescence probe H_2S-DDSY was used for *in vivo* near-infrared imaging of H_2S. To this end, both H_2S-DDSY (1 mM) and A4-β-Gals^{H363A} (0.005 mg/mL) were loaded into the HAMA hydrogel surrounding carotid arteries, and 100 μL of MeGal-DDSY (0.1 mg/mL) was then injected via the tail vein. All images were acquired using the "Cy5" filter with excitation at 640 nm (exposure time 800 ms; $n = 3$ for each group).

4.7. In vivo NO release

Electron paramagnetic resonance assay was employed to detect the release of NO in carotid artery as previously reported [12]. Briefly, one day after injection of the A4-β-Gals^{H363A}-loaded hydrogel around the carotid artery, mice were anesthetized with isoflurane. DETC sodium salt (500 mg/kg) was then administered via intraperitoneal injection in distilled deionized water (250 mM). Five minutes later, ammonium ferrous sulfate (50 mM) citrate solution (250 mM) was injected subcutaneously at a dosage of 2 mL/kg. Then, 100 μL MeGal-NO (0.1 mg/mL) was administered by tail vein injection. Thirty minutes later, carotid arteries were collected and frozen separately in liquid nitrogen. Subsequently, the frozen tissues were crumbled into small pieces in homogenizer tubes and extracted with ethyl acetate immediately. The ethyl acetate extract was then transferred to a 50 μL capillary tube and measured on x-band EPR. The EPR instrument was operated with the following settings: modulation frequency of 100 kHz, microwave power of 10 mW, modulation amplitude of 2 G, and 30 scans. The double integrated area of the EPR spectrum was standardized to determine the concentrations of NO-Fe(DETC)$_2$ using TEMPO as a reference.

4.8. Measurement of plasma H_2S and NOx level

For the measurement of H_2S and NOx levels, plasma samples was collected from mice after different treatments. H_2S levels were assessed using the methylene blue method. Briefly, 75 μL of plasma was mixed with 15 μL of $Zn(COO)_2$ solution (1 %, w/v), 30 μL of $FeCl_3$ solution (30 mM, dissolved in 1.2 M HCl), and 30 μL of N,N-dimethyl-*p*-phenylenediamine (20 mM, dissolved in 7.2 M HCl), the mixture was incubated for 20 min at 37 °C and centrifuged at 13000 *g* for 10 min. Finally, the absorbance was measured at 670 nm wavelength. Plasma NOx level was measured using a chemiluminescent analyzer (Sievers NOA 280i analyzer). Briefly, 25 μL of plasma was deproteinised by addition of 75 μL of ice-cold methanol. Then the mixture was centrifuged at 13000 *g* for 10 min at 4 °C, and 20 μL of the sample was added to 5 mL of vanadium (III) chloride (8 g/L, dissolved in 1 mol/L hydrochloric acid) refluxing at 95 °C under N_2.

4.9. Platelet preparation

Sprague-Dawley rats were deeply anesthetized, and blood was collected from the heart with sodium citrate (3.8 %) (9:1, v/v). To prevent platelet activation, blood was draw slowly and gently mixed with the anticoagulant by inverting the tube several times. Washed platelets were prepared as previously described [65]. The whole blood was centrifuged at 200 g for 8 min at room temperature, and the supernatant containing the platelets (platelet-rich plasma, PRP) was carefully collected from the upper portion. Subsequently, the collected PRP was centrifuged at 400 g for 10 min at room temperature. The platelet pellets were gently resuspended and washed with CGS buffer (120 mM NaCl, 12.9 mM trisodium citrate, and 30 mM glucose, pH 6.5), followed by centrifugation at 400*g* for 10 min at room temperature. The platelet pellets were resuspended in modified Tyrode buffer (134 mM NaCl, 0.34 mM NaH_2PO_4, 2.9 mM KCl, 12 mM $NaHCO_3$,20 mM HEPES, 2 mM $CaCl_2$, 1 mM $MgCl_2$, 10 mM glucose, pH 7.4). The purity of extracted platelets was assessed by flow cytometry [66]. Platelets were used within 2 h of isolation. The washed platelet was incubated for 30 min at 37 °C before use.

4.10. Platelet adhesion assay

In brief, 300 μL of collagen solution at a concentration of 0.012 mg/mL (dissolved in 0.006 M acetic acid) was added to each well of a 48-well plate, and incubated overnight. The coating solution was then removed, and the wells were washed twice with PBS buffer (pH 7.4). Subsequently, the wells were filled completely with 2 % (w/v) bovine serum albumin (BSA) diluted in PBS and incubated for 4 h at room temperature. The wells were washed twice with PBS buffer (pH 7.4) and air-dried before used for the adhesion assay. Next, washed rat platelets were added to the 48-well plate along with PBS buffer or "prodrugs-A4-β-Gals^{H363A} pair", and incubated at 37 °C for 30 min. The platelets were then fixed with 4 % paraformaldehyde. To increase the permeability of the cell membrane, adherent platelets were treated with 0.1 % Triton-X100 for 10 min. Subsequently, the platelets were incubated with phalloidin or primary antibody overnight at 4 °C, followed by incubation with secondary antibody at room temperature in the dark for 2 h. The adherent platelets were visualized using a confocal microscopy (Zeiss LSM710).

4.11. Clot retraction assay

The clot retraction assay was performed as previously documented [67]. At first, glass tubes were loaded with 745 μL of warm (30 °C) Tyrode's-Hepes buffer and 5 μL of red blood cells. Subsequently, rat platelet-rich plasma (PRP) was diluted with platelet-poor plasma (PPP) to standardize the platelet count to 2×10^8 cells/mL, 200 μL of PRP and 50 μL thrombin (20 U/mL) were added to each tube, along with PBS buffer or the A4-β-Gals^{H363A} and prodrugs-pair. The clots were retracted at 30 °C and imaged every 10 min for 2 h. The two-dimensional sizes of the retracted clots were analyzed using ImageJ software (NIH). The degree of retraction was presented as the clot area.

4.12. Maleimide assay

A modified biotin switch method using sulfhydryl-reactive Cy5.5-maleimide (red maleimide) was employed to evaluate the S-nitrosylation and S-sulfhydration levels of PDE5A with some adaptations as previously described [22,39]. The treated platelets were subjected to centrifugation at 3000*g* for 10 min, followed by resuspension in HEND buffer (250 mM HEPES-NaOH, 1 mM EDTA, 0.1 mM Neocuproine, and 0.1 mM Deferoxamine, pH 8.0) containing 20 mM N-ethylmaleimide (NEM) and 2.5 % SDS (w/v). The platelet suspension was incubated at 50 °C for 20 min with vortexing every 2 min. Subsequently, cold acetone was added to the sample, which was then incubated at −20 °C in the dark for 30 min before centrifugation at 3000*g*, 4 °C, for 15 min to remove the acetone. The protein pellets were resuspended in HEND buffer containing 1 % SDS (w/v) and divided into three portions: (1) incubated with 2 μM Cy5.5-maleimide at 4 °C for 2 h; (2) treated with 1 mM DTT at room temperature for 4 h, followed by solvent exchange with DTT-free HEND buffer through a 10 kDa ultrafiltration tube (Millipore Inc, USA), and then labeled with 2 μM Cy5.5-maleimide; (3) treated with 1 mM DTT at room temperature for 4 h, followed by solvent exchange with DTT-free HEND buffer, and incubated with 2 μM Cy5.5-maleimide and 1 mM Na-ascorbate.

PDE5A was enriched through immunoprecipitation. In brief, the sample was incubated with PDE5A antibody overnight in a rotating mixer. Subsequently, pre-prepared rProtein A/G plus Magpoly beads were added, and after 2 h of incubation at 4 °C, the beads were separated using a magnetic separator. The beads were then washed with a wash buffer (20 mM Na_2HPO_4, 0.15 M NaCl, pH 7.0) and the PDE5A was eluted with an elution buffer (0.1M glycine, pH 3.0). The protein concentration was determined using a BCA assay kit (PC0020, Solarbio), and the sample was subjected to gel electrophoresis. Finally, the gel was imaged using a fluorescence imaging system with a red excitation light and a 609 nm filter. The red fluorescence intensity of PDE5A was quantified using ImageJ software, and the ratio of fluorescence intensity to the input of PDE5A was utilized to evaluate the S-nitrosylation and S-sulfhydration levels of PDE5A.

4.13. Western blot

The treated platelets were lysed by multiple freeze-thaw cycles, after which the lysates were centrifuged at 12000 rpm and 4 °C for 15 min. The protein concentrations in the resulting supernatant were determined by a BCA assay kit. Subsequently, the samples were boiled in water for 10 min, separated on a 10 % SDS-PAGE gel, and transferred onto PVDF membranes (IPVH00010, Millipore). The membranes were blocked in 5 % non-fat milk for 1 h at room temperature and then incubated overnight at 4 °C with primary antibodies. Next, the membranes were washed six times with PBS buffer containing 0.1 % Tween and then incubated with the secondary antibodies at room temperature for 2 h. Immunoreactivity was detected using a chemiluminescent Western blotting detection kit (WBKLS0500, Millipore, Merck). The expression levels of the target proteins were normalized to β-actin.

4.14. Tail bleeding assay

The bleeding assay was performed as previously described with some modifications [68]. A total of 35 mice were randomly divided into 7 groups. Twenty μL of A4-β-Gals^{H363A}-loaded hydrogel was injected around the left carotid artery of the mice except for the sham group. Subsequently, the mice were administered with saline or prodrug solutions via tail vein injection as follows: (1) sham group, 100 μL of saline;

(2) Saline group, 100 μL of saline; (3) MeGal-H_2S group, 100 μL of MeGal-H_2S (0.424 mg/mL); (4) MeGal-NO group, 100 μL of MeGal-NO (0.103 mg/mL); (5) MeGal-(H_2S + NO) group, 50 μL of MeGal-NO (0.206 mg/mL) and 50 μL of MeGal-H_2S (0.848 mg/mL). (6) Gal-H_2S group, 100 μL of Gal-H_2S (0.412 mg/mL); (7) Gal-NO group, 100 μL of Gal-NO (0.1 mg/mL); Following this, the tails of the mice were transected 5 mm from the tip, and blood was blotted onto filter paper every 30 s until the paper was no longer stained with blood.

4.15. Mouse carotid artery thrombosis model

The ferric chloride-induced murine carotid arterial injury was performed as previously described with some modifications [69]. Mice were anesthetized with isoflurane and positioned in a supine orientation. The hair from the mouse's neck was shaved, and the skin along the midline of the neck was incised. Subsequently, the left carotid artery was separated, and the surrounding lateral fascia was carefully dissected using fine forceps. To block background fluorescence, a black plastic plate (3 × 4 mm) was positioned beneath the carotid artery. Next, 100 μL of Rhodamine 6G solution (0.5 mg/mL) was injected via the tail vein to label the blood cells. A piece of filter paper (1 × 2 mm) saturated with fresh 10 % $FeCl_3$ solution was picked up with a fine tip and placed directly on the carotid artery. After 5 min, the filter paper was removed, and the residual $FeCl_3$ was washed away with saline. Subsequently, 20 μL of A4-β-$Gals^{H363A}$-loaded hydrogel was injected immediately around the carotid artery, and 100 μL of saline or prodrug solutions were administered via tail vein injection. The blood flow was monitored under a fluorescence microscope (Leica M165FC), with images recorded at 1-min intervals until the blood flow was obstructed by a thrombus and the carotid artery ceased pulsating.

The mice were randomly divided to 4 groups by receiving various treatments: (1) saline group, 100 μL of saline; (2) MeGal-H_2S group, 100 μL of MeGal-H_2S (0.424 mg/mL); (3) MeGal-NO group, 100 μL of MeGal-NO (0.103 mg/mL); (4) MeGal-(H_2S + NO) group, 50 μL of MeGal-H_2S (0.848 mg/mL) and 50 μL of MeGal-NO (0.206 mg/mL).

4.16. Mouse deep vein thrombosis model

Flow reduction in the inferior vena cava (IVC) was accomplished as previously described [40]. The mice were anesthetized with isoflurane and positioned in a supine orientation. Following laparotomy, the intestines were carefully exposed, and sterile saline was continuously applied throughout the procedure to prevent drying. The IVC was gently separated from the aorta, and all visible side branches were ligated. Subsequently, ligation of the IVC was conducted over a 30 G needle (Jie Rui, Weihai, China), then the needle was removed and 20 μL of A4-β-$Gals^{H363A}$-loaded hydrogel was injected around the IVC. After surgery, peritoneum and skin were closed using 6-0 nylon sutures, followed by daily tail vein injection of saline or prodrug solutions.

Mice were randomly divided to 5 groups: (1) sham group, without any treatment; (2) saline group, 100 μL of saline; (3) MeGal-H_2S group, 100 μL of MeGal-H_2S (0.424 mg/mL); (4) MeGal-NO group, 100 μL of MeGal-NO (0.103 mg/mL); (5) MeGal-(H_2S + NO) group, 50 μL of MeGal-H_2S (0.848 mg/mL) and 50 μL of MeGal-NO (0.206 mg/mL). Mice were euthanized after 48 h, and the thrombi were collected for subsequent analysis.

4.17. Histological analysis of thrombus

At predetermined time points, mice were sacrificed and the thrombi were harvested. The thrombi were immediately rinsed with saline to remove residual blood. Following this, the thrombi were fixed in 4 % paraformaldehyde at room temperature for 20 min, embedded in OCT compound and cryo-sectioned (5 μm in thickness) (Leica CM 1950, Germany). Frozen sections were treated by histological H&E staining and periodic acid-schiff (PAS) staining according to the manufacturer's instructions. Images were acquired using a bright field microscope (Leica D-35578 Wetzlar, Germany), and the maximum ratio of the thrombus cross-sectional area was measured using ImageJ software.

4.18. Statistical analysis

All data are presented as the mean ± standard error of the mean (s.e.m) from a minimum of three independent experiments. Student's t-test was utilized for comparisons between two groups, while one-way or two-way analysis of variance (ANOVA) was employed for comparisons among more than two groups. Statistical analyses were performed using GraphPad Prism software 8.0 (GraphPad Software, San Diego, CA, USA) with statistical significance defined as $p < 0.05$.

CRediT authorship contribution statement

Weiliang Deng: Methodology, Investigation, Formal analysis, Data curation. **Zhixin Xu:** Investigation, Formal analysis, Data curation. **Tong Hua:** Investigation. **Guangbo Ji:** Methodology. **Zihang Wang:** Formal analysis. **Pei Liu:** Investigation. **Yupeng Zhang:** Data curation. **Shuo Li:** Methodology. **Yuqiu Chao:** Data curation. **Meng Qian:** Methodology, Investigation. **Qiang Zhao:** Writing – review & editing, Supervision, Funding acquisition, Conceptualization. **Jinwei Tian:** Writing – review & editing, Resources.

Data availability

All data needed to evaluate the conclusions in the paper are present in the paper and/or the Supplementary Materials. Additional data related to this paper may be requested from the authors.

Ethics approval and consent to participate

All experiments and animal procedures were approved by the Animal Experiments Ethical Committee of Nankai University (approval No. 20200037) and conducted in accordance with the *Guide for Care and Use of Laboratory Animals.*

Declaration of competing interest

The authors declare no conflict of interest.

Acknowledgement

This study was supported by grants from the National Natural Science Foundation of China (Nos. 81925021, 82330066, U21A20391, 823B2048, 82370343), Natural Science Foundation of Tianjin of China and the Natural Science Foundation of Heilongjiang Province of China (ZD2023H005).

Appendix A. Supplementary data

Supplementary data to this article can be found online at https://doi.org/10.1016/j.bioactmat.2025.02.012.

References

[1] B. Furie, B.C. Furie, Mechanisms of thrombus formation, N. Engl. J. Med. 359 (9) (2008) 938–949.
[2] A.M. Wendelboe, G.E. Raskob, Global burden of thrombosis, Circ. Res. 118 (9) (2016) 1340–1347.
[3] M. Koupenova, B.E. Kehrel, H.A. Corkrey, J.E. Freedman, Thrombosis and platelets: an update, Eur. Heart J. 38 (11) (2016) 785–791.
[4] N. Mackman, W. Bergmeier, G.A. Stouffer, J.I. Weitz, Therapeutic strategies for thrombosis: new targets and approaches, Nat. Rev. Drug Discov. 19 (5) (2020) 333–352.
[5] N. Mackman, Triggers, targets and treatments for thrombosis, Nature 451 (7181) (2008) 914–918.

[6] S. Calzavarini, R. Prince-Eladnani, F. Saller, L. Bologna, L. Burnier, A.C. Brisset, C. Quarroz, M.D. Reina Caro, V. Ermolayev, Y. Matsumura, J.A. Fernández, T. M. Hackeng, J.H. Griffin, A. Angelillo-Scherrer, Platelet protein S limits venous but not arterial thrombosis propensity by controlling coagulation in the thrombus, Blood 135 (22) (2020) 1969–1982.

[7] K. Huang, Z. Li, X. He, J. Dai, B. Huang, Y. Shi, D. Fan, Z. Zhang, Y. Liu, N. Li, Z. Zhang, J. Peng, C. Liu, R. Zeng, Z. Cen, T. Wang, W. Yang, M. Cen, J. Li, S. Yuan, L. Zhang, D. Hu, S. Huang, P. Chen, P. Lai, L. Lin, J. Wen, Z. Zhao, X. Huang, L. Yuan, L. Zhou, H. Wu, L. Huang, K. Feng, J. Wang, B. Liao, W. Cai, X. Deng, Y. Li, J. Li, Z. Hu, L. Yang, J. Li, Y. Zhuo, F. Zhang, L. Lin, Y. Luo, W. Zhang, Q. Ni, X. Hong, G. Chang, Y. Zhang, D. Guan, W. Cai, Y. Lu, F. Li, L. Yan, M. Ren, L. Li, S. Chen, Gut microbial co-metabolite 2-methylbutyrylcarnitine exacerbates thrombosis via binding to and activating integrin α2β1, Cell Metab. 36 (3) (2024) 598–616.e9.

[8] R. SoRelle, Nobel Prize awarded to scientists for nitric oxide discoveries, Circulation 98 (22) (1998) 2365–2366.

[9] C. Farah, L.Y.M. Michel, J.-L. Balligand, Nitric oxide signalling in cardiovascular health and disease, Nat. Rev. Cardiol. 15 (5) (2018) 292–316.

[10] S. Gambaryan, The role of NO/sGC/cGMP/PKG signaling pathway in regulation of platelet function, Cells 11 (22) (2022) 3704.

[11] J. Loscalzo, Nitric oxide insufficiency, platelet activation, and arterial thrombosis, Circ. Res. 88 (8) (2001) 756–762.

[12] F. Wang, K. Qin, K. Wang, H. Wang, Q. Liu, M. Qian, S. Chen, Y. Sun, J. Hou, Y. Wei, Y. Hu, Z. Li, Q. Xu, Q. Zhao, Nitric oxide improves regeneration and prevents calcification in bio-hybrid vascular grafts via regulation of vascular stem/progenitor cells, Cell Rep. 39 (12) (2022) 110981.

[13] Z. Wang, Y. Lu, K. Qin, Y. Wu, Y. Tian, J. Wang, J. Zhang, J. Hou, Y. Cui, K. Wang, J. Shen, Q. Xu, D. Kong, Q. Zhao, Enzyme-functionalized vascular grafts catalyze in-situ release of nitric oxide from exogenous NO prodrug, J. Contr. Release 210 (2015) 179–188.

[14] M. Emerson, Hydrogen sulfide and platelets: a possible role in thrombosis, chemistry, Biochemistry and Pharmacology of Hydrogen Sulfide (2015) 153–162.

[15] G. Cirino, C. Szabo, A. Papapetropoulos, Physiological roles of hydrogen sulfide in mammalian cells, tissues, and organs, Physiol. Rev. 103 (1) (2023) 31–276.

[16] G. Zagli, R. Patacchini, M. Trevisani, R. Abbate, S. Cinotti, G.F. Gensini, G. Masotti, P. Geppetti, Hydrogen sulfide inhibits human platelet aggregation, Eur. J. Pharmacol. 559 (1) (2007) 65–68.

[17] H. Nishikawa, H. Hayashi, S. Kubo, M. Tsubota-Matsunami, F. Sekiguchi, A. Kawabata, Inhibition by hydrogen sulfide of rabbit platelet aggregation and calcium mobilization, Biol. Pharm. Bull. 36 (8) (2013) 1278–1282.

[18] E. Grambow, F. Mueller-Graf, E. Delyagina, M. Frank, A. Kuhla, B. Vollmar, Effect of the hydrogen sulfide donor GYY4137 on platelet activation and microvascular thrombus formation in mice, Platelets 25 (3) (2014) 166–174.

[19] L. Zhong, L. Lv, J. Yang, X. Liao, J. Yu, R. Wang, P. Zhou, Inhibitory effect of hydrogen sulfide on platelet aggregation and the underlying mechanisms, J. Cardiovasc. Pharmacol. 64 (5) (2014) 481–487.

[20] R. d'Emmanuele di Villa Bianca, E. Mitidieri, M.N.D. Di Minno, N.S. Kirkby, T. D. Warner, G. Di Minno, G. Cirino, R. Sorrentino, Hydrogen sulphide pathway contributes to the enhanced human platelet aggregation in hyperhomocysteinemia, Proc. Natl. Acad. Sci. U. S. A 110 (39) (2013) 15812–15817.

[21] M.M. Cortese-Krott, G.G. Kuhnle, A. Dyson, B.O. Fernandez, M. Grman, J. F. DuMond, M.P. Barrow, G. McLeod, H. Nakagawa, K. Ondrias, P. Nagy, S.B. King, J.E. Saavedra, L.K. Keefer, M. Singer, M. Kelm, A.R. Butler, M. Feelisch, Key bioactive reaction products of the NO/H_2S interaction are S/N-hybrid species, polysulfides, and nitroxyl, Proc. Natl. Acad. Sci. U. S. A 112 (34) (2015) E4651–E4660.

[22] J. Sun, A.M. Aponte, S. Menazza, M. Gucek, C. Steenbergen, E. Murphy, Additive cardioprotection by pharmacological postconditioning with hydrogen sulfide and nitric oxide donors in mouse heart: S-sulfhydration vs. S-nitrosylation, Cardiovasc. Res. 110 (1) (2016) 96–106.

[23] C. Coletta, A. Papapetropoulos, K. Erdelyi, G. Olah, K. Módis, P. Panopoulos, A. Asimakopoulou, D. Gerö, I. Sharina, E. Martin, C. Szabo, Hydrogen sulfide and nitric oxide are mutually dependent in the regulation of angiogenesis and endothelium-dependent vasorelaxation, Proc. Natl. Acad. Sci. U. S. A 109 (23) (2012) 9161–9166.

[24] A. Degjoni, F. Campolo, L. Stefanini, M.A. Venneri, The NO/cGMP/PKG pathway in platelets: the therapeutic potential of PDE5 inhibitors in platelet disorders, J. Thromb. Haemostasis 20 (11) (2022) 2465–2474.

[25] X. Gui, X. Chu, Y. Du, Y. Wang, S. Zhang, Y. Ding, H. Tong, M. Xu, Y. Li, W. Ju, Z. Sun, Z. Li, L. Zeng, K. Xu, J. Qiao, Impaired platelet function and thrombus formation in PDE5A-deficient mice, Thromb. Haemost. 123 (2) (2022) 207–218.

[26] B. Lima, M.T. Forrester, D.T. Hess, J.S. Stamler, S-nitrosylation in cardiovascular signaling, Circ. Res. 106 (4) (2010) 633–646.

[27] J. Bai, F. Jiao, A.G. Salmeron, S. Xu, M. Xian, L. Huang, D.-b. Chen, Mapping pregnancy-dependent sulfhydrome unfolds diverse functions of protein sulfhydration in human uterine artery, Endocrinology 164 (9) (2023) 1–15.

[28] F. Krötz, H.Y. Sohn, U. Pohl, Reactive oxygen species, arterioscler, Thromb., Vasc. Biol. 24 (11) (2004) 1988–1996.

[29] C.t. Yang, N.O. Devarie-Baez, A. Hamsath, X.d. Fu, M. Xian, S-persulfidation: chemistry, chemical biology, and significance in health and disease, Antioxid. Redox Signaling 33 (15) (2020) 1092–1114.

[30] Y. Ge, F. Rong, W. Li, Y. Wang, On-demand therapeutic delivery of hydrogen sulfide aided by biomolecules, J. Contr. Release 352 (2022) 586–599.

[31] S.M. Andrabi, N.S. Sharma, A. Karan, S.M.S. Shahriar, B. Cordon, B. Ma, J. Xie, Nitric oxide: physiological functions, delivery, and biomedical applications, Adv. Sci. 10 (30) (2023) 2303259.

[32] J. Hou, Y. Pan, D. Zhu, Y. Fan, G. Feng, Y. Wei, H. Wang, K. Qin, T. Zhao, Q. Yang, Y. Zhu, Y. Che, Y. Liu, J. Cheng, D. Kong, P.G. Wang, J. Shen, Q. Zhao, Targeted delivery of nitric oxide via a 'bump-and-hole'-based enzyme–prodrug pair, Nat. Chem. Biol. 15 (2) (2019) 151–160.

[33] Q. Liu, G. Ji, Y. Chu, T. Hao, M. Qian, Q. Zhao, Enzyme-responsive hybrid prodrug of nitric oxide and hydrogen sulfide for heart failure therapy, Chem. Commun. 58 (53) (2022) 7396–7399.

[34] Y. Chen, R. Zhao, C. Tang, C. Zhang, W. Xu, L. Wu, Y. Wang, D. Ye, Y. Liang, Design and development of a bioorthogonal, visualizable and mitochondria-targeted hydrogen sulfide (H_2S) delivery system, Angew. Chem., Int. Ed. Engl. 61 (6) (2022) e202112734.

[35] X. Zhou, H. Wang, J. Zhang, X. Li, Y. Wu, Y. Wei, S. Ji, D. Kong, Q. Zhao, Functional poly(ε-caprolactone)/chitosan dressings with nitric oxide-releasing property improve wound healing, Acta Biomater. 54 (2017) 128–137.

[36] P.E.J. van der Meijden, J.W.M. Heemskerk, Platelet biology and functions: new concepts and clinical perspectives, Nat. Rev. Cardiol. 16 (3) (2019) 166–179.

[37] S. Gambaryan, A. Friebe, U. Walter, Does the NO/sGC/cGMP/PKG pathway play a stimulatory role in platelets? Blood 119 (22) (2012) 5335–5337.

[38] P. Wang, Q. Zhang, S. Li, B. Cheng, H. Xue, Z. Wei, T. Shao, Z.X. Liu, H. Cheng, Z. Wang, iCysMod: an integrative database for protein cysteine modifications in eukaryotes, Briefings Bioinf. 22 (5) (2021) 1–10.

[39] N. Sen, Bindu D. Paul, Moataz M. Gadalla, Asif K. Mustafa, T. Sen, R. Xu, S. Kim, Solomon H. Snyder, Hydrogen sulfide-linked sulfhydration of NF-κB mediates its antiapoptotic actions, Mol. Cell 45 (1) (2012) 13–24.

[40] A. Brill, T.A. Fuchs, A.K. Chauhan, J.J. Yang, S.F. De Meyer, M. Köllnberger, T. W. Wakefield, B. Lämmle, S. Massberg, D.D. Wagner, von Willebrand factor-mediated platelet adhesion is critical for deep vein thrombosis in mouse models, Blood 117 (4) (2011) 1400–1407.

[41] A. Yamashita, Y. Asada, Underlying mechanisms of thrombus formation/growth in atherothrombosis and deep vein thrombosis, Pathol. Int. 73 (2) (2023) 65–80.

[42] R. Hosoki, N. Matsuki, H. Kimura, The possible role of hydrogen sulfide as an endogenous smooth muscle relaxant in synergy with nitric oxide, Biochem. Biophys. Res. Commun. 237 (3) (1997) 527–531.

[43] A.L. King, D.J. Polhemus, S. Bhushan, H. Otsuka, K. Kondo, C.K. Nicholson, J. M. Bradley, K.N. Islam, J.W. Calvert, Y.X. Tao, Hydrogen sulfide cytoprotective signaling is endothelial nitric oxide synthase-nitric oxide dependent, Proc. Natl. Acad. Sci. U. S. A 111 (8) (2014) 3182–3187.

[44] Z. Li, H. Xia, T.E. Sharp, K.B. LaPenna, A. Katsouda, J.W. Elrod, J. Pfeilschifter, K.-F. Beck, S. Xu, M. Xian, T.T. Goodchild, A. Papapetropoulos, D.J. Lefer, Hydrogen sulfide modulates endothelial–mesenchymal transition in heart failure, Circ. Res. 132 (2) (2023) 154–166.

[45] D. Zhu, J. Hou, M. Qian, D. Jin, T. Hao, Y. Pan, H. Wang, S. Wu, S. Liu, F. Wang, L. Wu, Y. Zhong, Z. Yang, Y. Che, J. Shen, D. Kong, M. Yin, Q. Zhao, Nitrate-functionalized patch confers cardioprotection and improves heart repair after myocardial infarction via local nitric oxide delivery, Nat. Commun. 12 (1) (2021) 12.

[46] Q. Zong, J. Li, Q. Xu, Y. Liu, K. Wang, Y. Yuan, Self-immolative poly (thiocarbamate) with localized H_2S signal amplification for precise cancer imaging and therapy, Nat. Commun. 15 (1) (2024) 7558.

[47] B. He, Y. Zhang, H. Liu, M. Tang, K. Yang, S. Cheng, J. Shen, Y. Wei, W. Deng, Q. Zhao, G.Y. Yang, An endocellulase-triggered NO targeted-release enzyme-prodrug therapy system and its application in ischemia injury, Adv. Healthcare Mater. 13 (29) (2024) e2401599.

[48] A.C. Midgley, Y. Wei, Z. Li, D. Kong, Q. Zhao, Nitric-oxide-releasing biomaterial regulation of the stem cell microenvironment in regenerative medicine, Adv. Mater. 32 (3) (2020) 1805818.

[49] Y. Zheng, B. Yu, K. Ji, Z. Pan, V. Chittavong, B. Wang, Esterase-sensitive prodrugs with tunable release rates and direct generation of hydrogen sulfide, Angew. Chem., Int. Ed. Engl. 55 (14) (2016) 4514–4518.

[50] X. Wang, J. Shi, Z. Xu, D. Wang, Y. Song, G. Han, B. Wang, H. Cao, Y. Liu, J. Hou, Targeted delivery of nitric oxide triggered by α-glucosidase to ameliorate NSAIDs-induced enteropathy, Redox Biol. 59 (2023) 102590.

[51] J. Liu, Y. Bai, Y. Li, X. Li, K. Luo, Reprogramming the immunosuppressive tumor microenvironment through nanomedicine: an immunometabolism perspective, EBioMedicine 107 (2024) 105301.

[52] J. Liu, X. Li, Y. Li, Q. Gong, K. Luo, Metformin-based nanomedicines for reprogramming tumor immune microenvironment, Theranostics 15 (3) (2025) 993–1016.

[53] J. De Graaf, J. Banga, S. Moncada, R. Palmer, P. de Groot, J. Sixma, Nitric oxide functions as an inhibitor of platelet adhesion under flow conditions, Circulation 85 (6) (1992) 2284–2290.

[54] B. Brüne, K. Hanstein, Rapid reversibility of nitric oxide induced platelet inhibition, Thromb. Res. 90 (2) (1998) 83–91.

[55] L. Li, M. Whiteman, Y.Y. Guan, K.L. Neo, Y. Cheng, S.W. Lee, Y. Zhao, R. Baskar, C.-H. Tan, P.K. Moore, Characterization of a novel, water-soluble hydrogen sulfide–releasing molecule (GYY4137), Circulation 117 (18) (2008) 2351–2360.

[56] Z. Zhou, M. von Wantoch Rekowski, C. Coletta, C. Szabo, M. Bucci, G. Cirino, S. Topouzis, A. Papapetropoulos, A. Giannis, Thioglycine and l-thiovaline: biologically active H_2S-donors, Bioorg. Med. Chem. 20 (8) (2012) 2675–2678.

[57] B. Yu, Y. Zheng, Z. Yuan, S. Li, H. Zhu, L.K. De La Cruz, J. Zhang, K. Ji, S. Wang, B. Wang, Toward direct protein S-persulfidation: a prodrug approach that directly delivers hydrogen persulfide, J. Am. Chem. Soc. 140 (1) (2018) 30–33.

[58] J.M. Hare, J.S. Stamler, NO/redox disequilibrium in the failing heart and cardiovascular system, J. Clin. Investig. 115 (3) (2005) 509–517.

[59] R. Zoraghi, E.P. Bessay, J.D. Corbin, S.H. Francis, Structural and functional features in human PDE5A1 regulatory domain that provide for allosteric cGMP binding, dimerization, and regulation, J. Biol. Chem. 280 (12) (2005) 12051–12063.
[60] J. Wallis, Nitric oxide and blood: a review, Transfus, Médica Sur 15 (1) (2005) 1–11.
[61] J. Wittig, M.K. Drekolia, A. Kyselova, F.D. Lagos, M.L. Bochenek, J. Hu, K. Schäfer, I. Fleming, S.-I. Bibli, Endothelial-dependent S-Sulfhydration of tissue factor pathway inhibitor regulates blood coagulation, Redox Biol. 62 (2023) 102694.
[62] A. Morel, J. Malinowska, B. Olas, Hydrogen sulfide changes adhesive properties of fibrinogen and collagen in vitro, Platelets 25 (2) (2014) 147–149.
[63] M. Hidaka, S. Fushinobu, N. Ohtsu, H. Motoshima, H. Matsuzawa, H. Shoun, T. Wakagi, Trimeric crystal structure of the glycoside hydrolase family 42 β-galactosidase from Thermus thermophilus A4 and the structure of its complex with galactose, J. Mol. Biol. 322 (1) (2002) 79–91.
[64] A. Waterhouse, M. Bertoni, S. Bienert, G. Studer, G. Tauriello, R. Gumienny, F. T. Heer, T.A.P. de Beer, C. Rempfer, L. Bordoli, SWISS-MODEL: homology modelling of protein structures and complexes, Nucleic Acids Res. 46 (W1) (2018) W296–W303.
[65] A.L. Papa, A. Jiang, N. Korin, M.B. Chen, E.T. Langan, A. Waterhouse, E. Nash, J. Caroff, A. Graveline, A. Vernet, A. Mammoto, T. Mammoto, A. Jain, R.D. Kamm, M.J. Gounis, D.E. Ingber, Platelet decoys inhibit thrombosis and prevent metastatic tumor formation in preclinical models, Sci. Transl. Med. 11 (479) (2019) eaau5898.
[66] L. Yan, L. Zhou, B. Yan, L. Zhang, W. Du, F. Liu, Q. Yuan, P. Tong, L. Shan, T. Efferth, Growth factors-based beneficial effects of platelet lysate on umbilical cord-derived stem cells and their synergistic use in osteoarthritis treatment, Cell Death Dis. 11 (10) (2020) 857.
[67] K.L. Tucker, T. Sage, J.M. Gibbins, Clot retraction, Methods Mol. Biol. 788 (2012) 101–107.
[68] U.D.S. Sekhon, K. Swingle, A. Girish, N. Luc, M. de la Fuente, J. Alvikas, S. Haldeman, A. Hassoune, K. Shah, Y. Kim, S. Eppell, J. Capadona, A. Shoffstall, M.D. Neal, W. Li, M. Nieman, A. Sen Gupta, Platelet-mimicking procoagulant nanoparticles augment hemostasis in animal models of bleeding, Sci. Transl. Med. 14 (629) (2022) eabb8975.
[69] W. Li, T.M. McIntyre, R.L. Silverstein, Ferric chloride-induced murine carotid arterial injury: a model of redox pathology, Redox Biol. 1 (1) (2013) 50–55.